Sensing Coherent Dynamics of Electronic Spin Clusters in Solids

E. L. Rosenfeld, L. M. Pham, M. D. Lukin, and R. L. Walsworth

Phys. Rev. Lett. **120**, 243604 — Published 15 June 2018

DOI: 10.1103/PhysRevLett.120.243604

Sensing coherent dynamics of electronic spin clusters in solids

E. L. Rosenfeld[1], L. M. Pham[2], M. D. Lukin[1], and R. L. Walsworth[1,3*]
[1] *Department of Physics, Harvard University, Cambridge, Massachusetts 02138, USA*
[2] *MIT Lincoln Laboratory, Lexington, Massachusetts 02421, USA*
[3] *Harvard-Smithsonian Center for Astrophysics, Cambridge, Massachusetts 02138, USA*
(Dated: May 17, 2018)

We observe coherent spin exchange between identical electronic spins in the solid state, a key step towards full quantum control of electronic spin registers in room temperature solids. In a diamond substrate, a single nitrogen vacancy (NV) center coherently couples to two adjacent $S = 1/2$ dark electron spins via the magnetic dipolar interaction. We quantify NV-electron and electron-electron couplings via detailed spectroscopy, with good agreement to a model of strongly interacting spins. The electron-electron coupling enables an observation of coherent flip-flop dynamics between electronic spins in the solid state, which occur conditionally on the state of the NV. Finally, as a demonstration of coherent control, we selectively couple and transfer polarization between the NV and the pair of electron spins. Our observations enable the realization of fast quantum gate operations and quantum state transfer in a scalable, room temperature, quantum processor.

Introduction.—Measuring and manipulating coherent dynamics between individual pairs of electronic spins in the solid state opens a host of new possibilities beyond collective phenomena [1–5]. For example, a quantum register consisting of several coherently coupled electronic spins could serve as the basic building block of quantum information processors and quantum networks [6–8]. Additionally, recent proposals indicate that dynamics between many unpolarized electronic spins can mediate fully coherent coupling between distant qubits to be used for quantum state transfer [9–12]; measuring the coherent flip-flop rate between a pair of electronic spins could allow for sensitive distance measurements in individual molecules in nanoscale magnetic resonance imaging [13, 14].

However, such an interaction is a challenge to observe [13, 14]. In particular, the identical spins need to be close enough to interact strongly, such that the spins cannot be spatially or spectrally resolved, to allow for polarization exchange. In prior work, polarization transfer was measured between either spatially or spectrally resolved electronic spins: e.g., between two Strontium-88 ions separated by μm scales [15] or between a nitrogen vacancy (NV) color center and a substitutional nitrogen in diamond [16–19]. Conversely, nuclear spin-spin dynamics have been observed in diamond, facilitated by long nuclear spin coherence times and using a single NV center as a mediator [20–22]. Control of NV-nuclear spin clusters has led to using nuclear spins as a room temperature quantum memory and quantum register [22–25], with applications such as NMR detection of a single protein [26] and quantum networks [23, 27]. Similarly, manipulating interactions between identical electronic spins could lead to faster gate times and long-distance transport in solid state, room-temperature quantum information processors [9], features that are challenging for nuclear spins due to their weaker coupling strengths.

Here, we report coherent spin exchange between two identical electronic spins, a vital prerequisite for many of the ideas discussed above, including the aforementioned collective phenomena [1–5]. A single NV center acts as a nanoscale probe of flip-flop interactions between a pair of electron spins. First, we identify a coherently-coupled, three-spin cluster consisting of the optically-active NV and two optically-dark electron spins inside the diamond [Fig. 1(a)]. The coupling strengths and resonance frequencies for the three spins are extracted via optically detected magnetic resonance (ODMR) NV spectroscopy, as well as dynamical decoupling and double electron-electron resonance (DEER) experiments. The electron spins undergo flip-flop dynamics, conditional on the state of the NV [Fig. 1(b)], as in a controlled SWAP gate. Finally, we demonstrate partial manipulation of the three-electronic-spin cluster through selective coupling and transfer of polarization between the NV and the pair of electron spins.

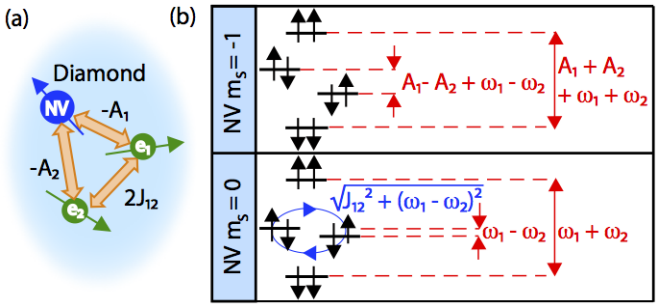

FIG. 1. (a) Schematic of a three-electronic-spin cluster in diamond, labeled with coupling strengths. (b) Energy level diagram of two dipolar-coupled dark electron spins (each S = 1/2) as a function of the nearby NV spin state (S = 1). When the NV is in the $|-1\rangle_{\rm NV}$ spin state, the magnetic field gradient it produces at the electrons suppresses their dynamics. When the NV is in the $|0\rangle_{\rm NV}$ spin state, flip-flops are allowed between the electron spins.

Experimental results.—The unpolished diamond sam-

* rwalsworth@cfa.harvard.edu

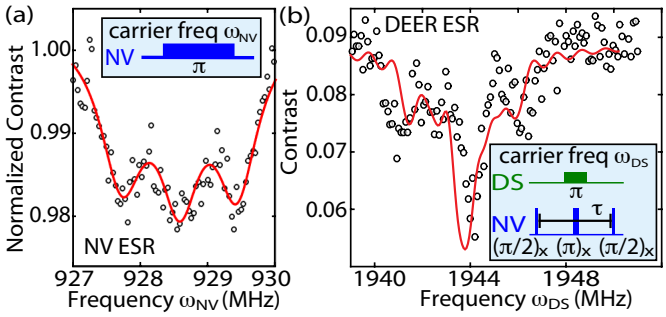

FIG. 2. Spectroscopy of three electronic-spin cluster. (a) Measured NV ESR spectrum (black circles), in the presence of a $B_0 = 694.0(6)$ G static bias field, fit to three Lorentzian curves (red line). The triplet-like structure is consistent with the model and parameter values presented in this work. The ^{14}N nuclear spin is polarized into the $m_I = +1$ state due to the large transverse NV-^{14}N hyperfine coupling in the optically excited manifold [28, 29]. The estimate of the B_0 field is adjusted accordingly. Inset, NV ESR pulse sequence. (b) DEER ESR spectrum data (black dots), in the presence of a $B_0 = 694.0(6)$ G bias field, with numerical simulation from equation (1) using parameter values given in the main text (red line). Time τ is fixed to 3 μs. Observed lineshape is qualitatively consistent with two electrons strongly coupled to both each other and the probe NV. Inset, DEER ESR pulse sequence.

ple features a 99.999% ^{12}C epitaxially grown layer, implanted with ^{14}N ions at 2.5 keV and annealed for eight hours at 900 °C. A mask implantation was performed, such that the density of implanted nitrogen varied from close to zero to 10^{12}/cm^2 across the sample. Measurements were performed using a custom-built confocal microscope with a 532 nm laser for NV excitation, and a single photon counter to collect phonon sideband photoluminescence for population readout of the NV ground state sublevels. A dual-channel arbitrary waveform generator enables coherent driving of the NV spin and two additional electron spins in the diamond. The NV and electron spin levels are split by a DC magnetic field ($B_0 = 694.0(6)$ G) aligned along the NV axis and generated by a permanent magnet.

An electron spin resonance (ESR) measurement on the NV reveals an atypical spectrum. Figure 2(a) illustrates the atypical ESR spectrum containing a triplet-like structure, with splitting about a factor of 2.5 smaller than the ^{14}N hyperfine coupling [30]. Fitting the data to three Lorentzian lineshapes demonstrates a full splitting of 1.70(7) MHz.

To determine if this characteristic splitting is explained by the presence of spins with electronic character, we selectively drive the spins with resonances around $\gamma_e B_0$, using a separate microwave channel (labeled DS for "dark spin" in Figure 2(b), inset). When the DS drive frequency approaches a resonance of an electron spin coupled to the NV, the NV Bloch vector accumulates phase in the transverse plane as in a Double-Electron-Electron-Resonance spectroscopy (DEER ESR) experiment. With a central dip around $g = 2$, the spectrum shows a characteristic, asymmetric lineshape [Fig. 2(b)], for which either nuclear quadrupolar spin(s) strongly coupled to a single electron, or dipolar coupling(s) between multiple electronic spins could be responsible.

Distinguishing between these possibilities requires a study of the number of electronic spins present. In a Spin Echo DOuble Resonance (SEDOR) pulse sequence [1] [Fig. 3(a), bottom panel], a single electron spin induces oscillations in the NV population, and hence the ODMR signal, at the frequency of the NV-electron dipolar coupling strength. However, the presence of multiple electronic spins results in multiple frequencies, originating from the different coupling strengths (electron-electron, NV-electron), as well as any coherent dynamics. The resulting data exhibits several frequency components [Fig. 3(b)], consistent with a coherently-coupled, multi-electronic spin system [Fig. 1(a)]. Comparing the observed Rabi frequencies of the NV and electronic spin transitions confirms that the dark electron spins are S = 1/2 [31].

Model and Hamiltonian.—The triplet lineshape components extracted from the NV ESR, as well as the frequencies in the SEDOR measurement [Fig. 3(b)], are well-described by a system of two electron spins coherently coupled to the NV. The three-spin cluster is modeled using the following Hamiltonian, in the secular approximation and frame rotating at the NV transition frequency:

$$\frac{\mathcal{H}}{h} = \sum_{i=1,2} \Big(\omega_i + A_i(S_z^{\rm NV} + \mathbf{I}/2)\Big) S_z^{(i)} + J_{12}\Big(2S_z^{(1)}S_z^{(2)} - \frac{1}{2}(S_+^{(1)}S_-^{(2)} + S_-^{(1)}S_+^{(2)})\Big). \quad (1)$$

Here, $-A_i h = -\mu_0 \hbar^2 \gamma_e^2 (3\cos^2\theta_i - 1)/(4\pi r_i^3)$ is the magnetic dipole interaction strength between the NV and electron i. The electron-electron coupling term $J_{12}h = -\mu_0\hbar^2\gamma_e^2(3\cos^2\theta_{12} - 1)/(8\pi r_{12}^3)$ is half the magnetic dipole interaction strength between the electrons, and ω_i is the Zeeman energies of electron i. Note that the $|m_s = +1\rangle \equiv |+1\rangle_{\rm NV}$ state is not populated under the experimental conditions employed in this work, reducing the NV subspace to $|0\rangle_{\rm NV}$ and $|-1\rangle_{\rm NV}$ in equation (1). Therefore, all of the operators are 2x2 spin matrices.

An analytical calculation of the SEDOR signal using the Hamiltonian in equation 1 yields four characteristic frequencies (labeled Δ_{1-4}), which are functions of J_{12}, $A_1 - A_2$, and $\omega_1 - \omega_2$ [31]. We find good agreement between the SEDOR data and a sum of four sine waves (one of which is below the spectral resolution of the current experiment), multiplied by $e^{-(t/T_2)^p}$ to account for NV decoherence [Fig. 3(b)]. To extract the parameter values, we associate the three resolved frequencies with the predicted frequency-domain behavior from the model [31] and solve for J_{12}, $\omega_1\omega_2$ and $A_1 - A_2$, obtaining an upper bound on $A_1 + A_2$ from the unresolved frequency compo-

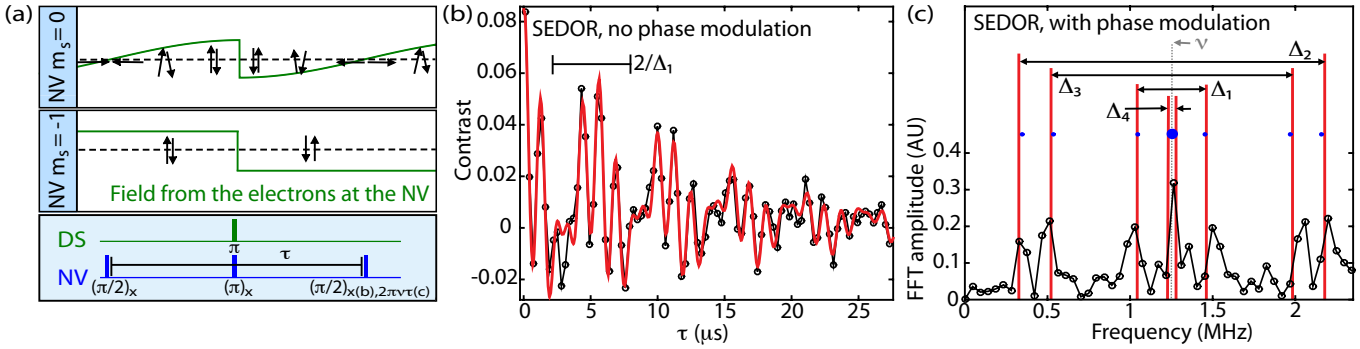

FIG. 3. Coherent dynamics of the three-electronic-spin cluster. (a) Lowest panel: SEDOR pulse sequence schematic. Uppermost panel: depiction of the electron dynamics corresponding to NV population in $|0\rangle_{\rm NV}$. Middle panel: electron spin evolution corresponding to $|-1\rangle_{\rm NV}$. (b) Time-domain data (black circles and line) of the SEDOR experiment. The solid red line is a fit to four sine waves multiplied by a decaying exponential ($T_2 = 14(3)$ μs, p = 1.1(4)). The frequencies from the fit are consistent with the frequencies reported with the model and parameter values [31]. The period $2/\Delta_1$ corresponding to the electron flip-flop dynamics is shown. Data was taken at 180 G. (c) Fourier transform of data from the SEDOR experiment performed with phase modulation (TPPI) on the last NV $\pi/2$ pulse at a frequency $\nu = 1.25$ MHz (black dots and line). The signal amplitudes for each frequency pair about ν are equal, consistent with two unpolarized electron spins. Blue dots correspond to the frequencies found in the fit in (b), up-converted by the TPPI frequency ν. Error bars (95% CI) from the fit are a factor of four smaller than the diameter of the dots, except for the large dot at ν, for which the error is the size of the dot. The vertical red lines represent frequency components Δ_{1-4} corresponding to the analytical solution using the model and parameter values reported in the main text [31].

nent. We impose agreement with the observed NV ESR and DEER ESR spectrum to confirm our solution and inform the value of ω_1, as well as the value of $A_1 + A_2$ [31]. The resulting parameter values reported here are $A_{1,2} = 0.81(5), -0.86(5)$ MHz; $J_{12} = \pm 0.38(5)$ MHz; $\omega_1 = \gamma_e B_0 + 0(2)$ MHz and $\omega_2 = \omega_1 - 0.14(5)$ MHz [31].

As mentioned above, this model is also consistent with the observed NV ESR and DEER ESR spectra [Fig. 2]. Two of the eigenstates of the electron pair, $|\uparrow\downarrow\rangle$, $|\downarrow\uparrow\rangle$, each induce a dipolar magnetic field of strength $\pm(A_1 - A_2)/2 = \pm 0.84(4)$ MHz, which consequently splits the NV ESR lines. The two other electron pair states, $|\downarrow\downarrow\rangle$ and $|\uparrow\uparrow\rangle$, exert a field with strength $\pm(A_1 + A_2)/2 = \pm 0.03(4)$ MHz. The result is an NV triplet-like spectrum, with splittings given by the difference of the NV-electron couplings. As mentioned above, fitting the NV ESR data [Fig. 2(a), black dots] to a sum of three Lorentzian curves confirms the NV resonance frequencies, which are split by 1.70(7) MHz (95% CI of the fit), in good agreement with the model parameters $A_1 - A_2 = 1.67(7)$ MHz.

Conversely, the presence of multiple electrons corrupts the direct measurement of individual transition frequencies in the DEER ESR spectrum. The DEER ESR lineshape depends sensitively on all coupling and resonance frequency parameters [31], which we calculate numerically with the model. Using the same parameter values listed above, we demonstrate good qualitative agreement between the DEER ESR data [Fig. 2(b), black dots] and the model [Fig. 2(b), red line], within the error ranges on the extracted model parameters [31].

Coherent dynamics in the cluster.—An understanding of the three-electronic-spin cluster allows for a discussion of the coherent dynamics between the electron spins. When the $|-1\rangle_{\rm NV}$ spin state is occupied, two of the electron-pair energy levels, $|\uparrow\downarrow\rangle$ and $|\downarrow\uparrow\rangle$, differ by $A_1 - A_2 + \omega_1 - \omega_2 = 1.81(9)$ MHz, which is larger than their coupling strength $J_{12} = \pm 0.38(5)$ MHz; thus, flip-flops are suppressed [Fig. 1(c), top panel]. However, when the NV population occupies the $|0\rangle_{\rm NV}$ spin state, the same two energy levels are split by only $\omega_1 - \omega_2 = 0.14(5)$ MHz, allowing for polarization exchange [Fig. 1(c), bottom panel]. Direct diagonalization of the Hamiltonian shows that flip-flops occur at rate $\Delta_1 \equiv \sqrt{J_{12}^2 + (\omega_1 - \omega_2)^2} = 0.41(5)$ MHz [Fig. 1(b), bottom panel].

In the SEDOR pulse sequence, sweeping the free precession time τ and fixing the electron spin π-pulse on resonance allows for quantitative observations of the flip-flop frequency between the electrons. During the time τ, the NV Bloch vector accumulates phase in the transverse plane due to the dipolar field of the electrons, described by the $S_z^{\rm NV} S_z^{(i)}$ terms in equation (1). Since half of the NV population is in the $|0\rangle_{\rm NV}$ spin state throughout this measurement, dynamics between the pair of electrons are partially allowed [Fig. 3(a), top and middle panels]. Sweeping the free precession time constitutes an AC magnetometer, where the AC field amplitude of 0.84(4) MHz is generated by the pair of electrons in the $|\uparrow\downarrow\rangle$ or $|\downarrow\uparrow\rangle$ states. The detected AC field frequency $\Delta_1/2$ is given by half the electron spin pair flip-flop rate [Fig. 3(a), top panel], and is marked in the time domain in Figure 3(b). As constructed, the frequency components of the SEDOR data implies $\Delta_1 = 0.41(5)$ MHz, equal to the value found with the model parameters [31].

In addition, the parameters A_1 and A_2 contribute to other frequency components. During the SEDOR se-

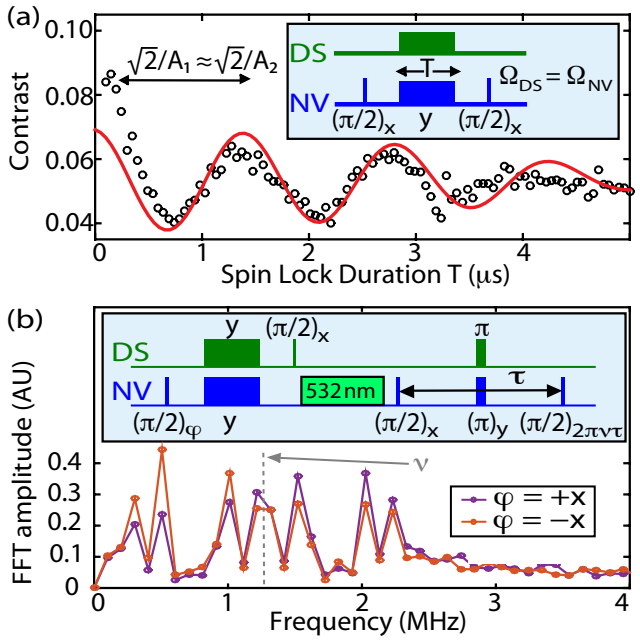

FIG. 4. Coherent polarization transfer between the NV and two dark electron spins. (a) Observed polarization transfer to the electrons at the Hartmann-Hahn resonance condition [37] as a function of spin lock duration T (black circles). Red line is a numerical simulation of the experiment protocol using equation (1) and the parameter values given in the main text. The primary oscillation frequency of 0.60(5) MHz, $\simeq A_1/\sqrt{2} \simeq A_2/\sqrt{2}$, is consistent with the two similar NV-electron coupling strengths adding in quadrature. Due to microwave amplitude instability of the setup, we allow for a detuning from the resonance condition up to 350 kHz. Effects not included in our model that contribute to the deviation at short T are: slow drifts in this detuning, dephasing of detuned driving of (weakly populated) hyperfine transitions, and pulse errors of the initial NV $\pi/2$ pulse. Inset, Hartmann-Hahn pulse sequence. (b) Observed polarization transfer to the electrons using Hartmann-Hahn cross polarization at fixed spin lock duration T = 700 ns, followed by optical repolarization of the NV to $|0\rangle_{\rm NV}$, then readout of the electron pair polarization via SEDOR. Results are displayed as the FFT of the SEDOR data. The phase ϕ of the first NV pulse determines the direction of polarization transfer. For both directions, the polarization is shared across the three frequency pairs, consistent with two coupled electron spins. Inset, experimental pulse sequence.

quence, the other half of the NV population occupies the $|-1\rangle_{\rm NV}$ spin state, such that the electron-pair dynamics are suppressed by the field of strength $A_1 - A_2 = 1.67(7)$ MHz [Fig. 3(a), middle panel]. The eigenstates of the relevant Hamiltonian $H_{-1}^{\rm DS}$ are mostly described by the Zeeman $|\uparrow\downarrow\rangle$ and $|\downarrow\uparrow\rangle$ states, and are dressed by their interaction, which shifts their energy splitting. These states consequently modulate the SEDOR data at rate $\frac{1}{2}\sqrt{(A_1 - A_2 + \omega_1 - \omega_2)^2 + J_{12}^2} \equiv \Delta_2/2 = 0.93(4)$ MHz, equal to a frequency component observed in the SEDOR data [31].

Throughout the pulse sequence, the NV is in a coherent superposition of the $|0\rangle_{\rm NV}$ and $|-1\rangle_{\rm NV}$ spin states. The resulting interference of both electron propagators induces additional frequency components in the NV evolution at half the sums and differences of Δ_1 and Δ_2 [31]. We find that the amplitude of the $(\Delta_1 + \Delta_2)/2$ frequency component decreases via destructive interference of the two propagator paths, due to the relative detuning between the two electrons $\omega_1 - \omega_2$ [31]; similarly, the amplitude of the $(\Delta_2 - \Delta_1)/2 \equiv \Delta_3/2 = \frac{1}{2}(\sqrt{(A_1 - A_2 + \omega_1 - \omega_2)^2 + J_{12}^2} - \sqrt{J_{12}^2 + (\omega_1 - \omega_2)^2}) = 0.72(2)$ MHz component increases [31]. As expected, the fit to the SEDOR data also exhibits a frequency component at 0.72(2) MHz [31]. Finally, irrespective of the state of the NV, the states $|\uparrow\uparrow\rangle$ and $|\downarrow\downarrow\rangle$ modulate the SEDOR signal at the frequency $\Delta_4/2 \equiv (A_1 + A_2)/2$. For the present three-spin system, we estimate $\Delta_4/2 = -0.03(4)$ MHz, which is not distinguishable from zero for the present experiment.

As a check of reproducibility, we repeat the SEDOR experiment using a phase modulation technique [31], known as time-proportional phase increments (TPPI) in nuclear magnetic resonance, to up-convert the signals away from zero frequency by $\nu = 1.25$ MHz [1] [Fig. 3(c)]. The Fourier transform of the TPPI data [Fig. 3(c), black line] shows pairs of spectral peaks at frequencies corresponding to Δ_{1-3}, centered around the TPPI frequency ν; as before, the Δ_4 peaks are not resolved. The positive and negative frequency components of each pair have approximately equal amplitude, consistent with unpolarized electron spins. The red lines corresponding to Δ_{1-4} in Figure 3(c) indicate the expected frequencies from model. The frequency components from the fit of the time domain data [Fig. 3(b)] are up-converted by ν and marked as blue dots, and agree with the model within the margin of error [31].

Manipulation of the electronic spins.—Finally, we demonstrate coherent manipulation of the three-spin cluster by transferring polarization from the NV to the dark electron spin pair using a Hartmann-Hahn technique [37]. We first fix the amplitude of the drives to the Hartmann-Hahn resonance condition [37], and transfer polarization from the NV to the electron spins while sweeping the spin lock duration T [Fig. 4(a)]. By matching the dressed state energies of the NV and dark spins, NV-dark spin flip-flops become allowed and the dark spins are polarized. By energy conservation, the dark spins are aligned parallel (anti-parallel) to the resonant drive vector in the rotating frame, if the NV Bloch vector is initialized parallel (anti-parallel) along the NV drive vector. The polarization evolves from the NV and returns at a rate approximately given by $A_1/\sqrt{2} \approx A_2/\sqrt{2}$, as expected for two uncorrelated electrons with approximately equal coupling to the NV. Next, we observe polarization of the dark electron spin pair by fixing the spin lock duration at T = 700 ns $\approx 1/|\sqrt{2}A_1| \approx 1/|\sqrt{2}A_2|$, re-polarizing the NV with a 532 nm laser pulse, and reading out the polarization of the electron spins using SEDOR and TPPI. Changing the phase of the first $\pi/2$ pulse on the NV,

and therefore the initial NV dressed state, exchanges the direction of polarization transfer [Fig. 4(b), orange and purple lines]. Adding a $\pi/2$ pulse on the dark spins after the spin lock pulse stores the dark spin polarization along the quantization axis. For both polarization transfer directions, the difference in peak amplitude is spread across all pairs of frequencies Δ_{1-3} [Fig. 4(b)], as is expected for a coupled pair of electrons. Compared to previous work [18, 19], this constitutes a measurement of coherent polarization transfer from the NV to electron spins, followed by readout of the polarization, opening the door to quantitative estimates of dark spin state preparation fidelities. Here, a careful study of the polarization fidelity will require stringent microwave amplitude stability during a two-dimensional sweep of T and τ, beyond the scope of this work.

Outlook.— Our observations of coherent dynamics between nearby electronic spins in the solid state, under ambient conditions and without spectrally or spatially resolved spins, constitutes a key step toward realizing coherent quantum manipulation of electronic spins. Specifically, the demonstrated techniques can be used to implement quantum registers with fast gate time and quantum state transfer between remote spins via an intermediate spin bath [9–12]. Additionally, electronic spin dynamics external to an NV could enable a range of potential sensing applications. For example, it can be employed following a recent proposal to measure the spin diffusion rate between intra-molecular spin labels in biomolecules [13, 14], to obtain improved distance measurements beyond the standard DEER protocol [38, 39].

We are indebted to R. Landig, S. Choi, D. Bucher, A. Sushkov, H. Knowles, J. Gieseler, P. Cappellaro, T. van der Sar, E. Bauch, C. Hart, M. Newton and B. Green for fruitful discussions, and especially A. Cooper for informing the authors about the phase modulation technique. The authors are grateful to J. Lee for fabricating the microwave stripline and A. Ajoy for implanting the diamond sample. E. R. acknowledges financial support from the NSF. This work was performed in part at the Center for Nanoscale Systems (CNS), a member of the National Nanotechnology Coordinated Infrastructure Network (NNCI), which is supported by the National Science Foundation under NSF award no. 1541959. CNS is part of Harvard University. This material is based upon work supported by, or in part by, the U. S. Army Research Laboratory and the U. S. Army Research Office under contract/grant numbers W911NF1510548 and W911NF1110400. This work was additionally supported by the NSF, CUA, Vannever Bush Faculty Fellowship and Moore Foundation.

[1] Arthur Schweiger and Gunnar Jeschke, *Principles of Pulse Electron Paramagnetic Resonance* (Oxford University Press, 2001).
[2] S. Clough and C.A. Scott, J. Phys. C: Solid State Phys. **1** 919 (1968).
[3] A. M. Tyryshkin, S. Tojo, J. J. L. Morton, H. Riemann, N. V. Abrosimov, P. Becker, H. Pohl, T. Schenkel, M. L. W. Thewalt, K. M. Itoh and S. A. Lyon, Nat. Mater. **11**, 143-147 (2012).
[4] J. Choi, S. Choi, G. Kucsko, P. C. Maurer, B. J. Shields, H. Sumiya, S. Onoda, J. Isoya, E. Demler, F. Jelezko, N. Y. Yao and M. D. Lukin, Phys. Rev. Lett, **118**, 093601 (2017).
[5] G. Kucsko, S. Choi, J. Choi, P. C. Maurer, H. Sumiya, S. Onoda, J. Isoya, F. Jelezko, E. Demler, N. Y. Yao and M. D. Lukin, arXiv:1609.08216
[6] P. Neumann, R. Kolesov, B. Naydenov, J. Beck, F. Rempp, M. Steiner, V. Jacques, G. Balasubramanian, M. L. Markham, D. J. Twitchen, S. Pezzagna, J. Meijer, J. Twamley, F. Jelezko and J. Wrachtrup, Nat. Phys. **6**, 249-253 (2010).
[7] P. Cappellaro, L. Jiang, J. S. Hodges and M. D. Lukin, Phys. Rev. Lett. **102**, 210502 (2009).
[8] P. Neumann, N. Mizuochi, F. Rempp, P. Hemmer, H. Watanbe, S. Yamasaki, V. Jacques, T. Gaebel, F. Jelezko and J. Wrachtrup, Science **320** 5881 (2008).
[9] N. Y. Yao, L. Jiang, A. V. Gorshkov, Z.-X. Gong, A. Zhai, L.-M. Duan, and M. D. Lukin, Phys. Rev. Lett. **106**, 040505 (2011).
[10] A. Ajoy and P. Cappellaro, Phys. Rev. B **87**, 064303 (2013).
[11] G. Gualdi, V. Kostak, I. Marzoli, and P. Tombesi, Phys. Rev. A **78**, 022325 (2008).
[12] P. Cappellaro in *Quantum State Transfer and Network Engineering*, (Springer, Berlin, Heidelberg, 2014).
[13] A. Blank, Phys. Chem. Chem. Phys., **19**, 5222, (2017).
[14] E. Dikarov, O. Zgadzai, Y. Artzi, and A. Blank, Phys. Rev. Applied **6**, 044001 (2016).
[15] S. Kotler, N. Akerman, N. Navon, Y. Glickman and R. Ozeri, Nature **510**, 376380 (2014).
[16] T. Gaebel, M. Domhan, I. Popa, C. Wittmann, P. Neumann, F. Jelezko, J. R. Rabeau, N. Stavrias, A. D. Greentree, S. Prawer, J. Meijer, J. Twamley, P. R. Hemmer and J. Wrachtrup, Nat. Phys. **2**, 408-413 (2006).
[17] R. Hanson, F. M. Mendoza, R. J. Epstein, and D. D. Awschalom, Phys. Rev. Lett **97**, 087601 (2006).
[18] H. S. Knowles, D. M. Kara, and M. Atature, Phys. Rev. Lett. **117**, 100802 (2016).
[19] C. Belthangady, N. Bar-Gill, L. M. Pham, K. Arai, D. Le Sage, P. Cappellaro, and R. L. Walsworth, Phys. Rev. Lett. **110**, 157601 (2013).
[20] L. Childress , M. V. Gurudev Dutt, J. M. Taylor, A. S. Zibrov, F. Jelezko, J. Wrachtrup, P. R. Hemmer, and M. D. Lukin, Science **314**, 5797 (2006).
[21] M. V. Gurudev, L. Childress, L. Jiang, E. Togan, J. Maze, F. Jelezko, A. S. Zibrov, P. R. Hemmer, and M. D. Lukin, Science **316**, 5829 (2007).
[22] L. Jiang, J. S. Hodges, J. R. Maze, P. Maurer, J. M. Taylor, D. G. Cory, P. R. Hemmer, R. L. Walsworth, A. Yacoby, A. S. Zibrov, and M. D. Lukin, Science **326**, 5950 (2009).
[23] T. H. Taminiau, J. Cramer, T. van der Sar, V. V. Do-

brovitski, and R. Hanson, Nat. Nanotechnol. **9**, 171-176 (2014).
[24] N. Kalb, J. Cramer, D. J. Twitchen, M. Markham, R. Hanson, and T. H. Taminiau, Nat. Comm. **7**, 13111 (2016).
[25] M. H. Abobeih, J. Cramer, M. A. Bakker, N. Kalb, M. Markham, D. J. Twitchen, and T. H. Taminiau, arXiv: 1801.01196.
[26] I. Lovchinsky, A. O. Sushkov, E. Urbach, N. P. de Leon, S. Choi, K. De Greve, R. Evans, R. Gertner, E. Bersin, C. Muller, L. McGuinness, F. Jelezko, R. L. Walsworth, H. Park, and M. D. Lukin, Science **351** 6275 (2016).
[27] A. Reiserer, N. Kalb, M. S. Blok, K. J. M. van Bemmelen, T. H. Taminiau, R. Hanson, D. J. Twitchen, and M. Markham, Phys. Rev. X **6**, 021040 (2016).
[28] R. Fischer, A. Jarmola, P. Kehayias, and D. Budker, Phys. Rev. B **87**, 125207 (2013).
[29] V. Jacques, P. Neumann, J. Beck, M. Markham, D. Twitchen, J. Meijer, F. Kaiser, G. Balasubramanian, F. Jelezko, and J. Wrachtrup, Phys. Rev. Lett. **102**, 057403 (2009).
[30] S. Felton, A. M. Edmonds, M. E. Newton, P. M. Martineau, D. Fisher, D. J. Twitchen, and J. M. Baker, Phys. Rev. B, **79**, 075203 (2009).
[31] Supplemental Material available at *url*, which includes Refs. [32–36]
[32] M. D. Calin, E. Helerea, Temperature Influence on Magnetic Characteristics of NdFeB Permanent Magnets (IEEE, Bucharest, Romania, 2011).
[33] B. Green, M. Dale and M. Newton, Phys. Rev. B **82**, 165204 (2015).
[34] C. Glover, P. Martineau, D. Twitchen, and J. Baker, Phys. Rev. Lett. **90**, 18 (2003).
[35] O. Tucker, M. Newton and J. Baker, Phys. Rev. B **50**, 21 (1994).
[36] A. O. Sushkov, I. Lovchinsky, N. Chisholm, R. L. Walsworth, H. Park and M. D. Lukin, Phys. Rev. Lett. **113**, 197601 (2014).
[37] S. R. Hartmann and E. L. Hahn, Phys. Rev **128**, 2042 (1962).
[38] G. Jeschke, Annu. Rev. Phys. Chem., **63**, 419446 (2012).
[39] G. Jeschke, M. Pannier and W. Spiess in *Distance Measurements in Biological Systems by EPR*, (Springer, Boston, MA, 2006) 19, 493-512.